Journal of Quantitative Spectroscopy & Radiative Transfer 296 (2023) 108451

Contents lists available at ScienceDirect

Journal of Quantitative Spectroscopy & Radiative Transfer

journal homepage: www.elsevier.com/locate/jqsrt

Electromagnetic coupling and determination of the structure factor of fractal aggregates

Clément Argentin[a], Matthew J. Berg[b], Marek Mazur[a], Romain Ceolato[c], Jérôme Yon[a,*]

[a] Normandie Univ, UNIROUEN, INSA Rouen, CNRS, CORIA, 76000 Rouen, France
[b] Kansas State University, Department of Physics, 1228 N. Martin Luther King Jr. Dr., Manhattan, KS 66506-2601, USA
[c] ONERA, The French Aerospace Lab, Université de Toulouse, FR 31055, France

ARTICLE INFO

Article history:
Received 28 June 2022
Revised 27 November 2022
Accepted 29 November 2022
Available online 30 November 2022

Keywords:
Soot fractal aggregates
Structure factor
RDG-FA
Internal coupling
DDA
Phasor analysis
Autocorrelation
Light scattering

ABSTRACT

The Rayleigh-Debye-Gans approximation for fractal aggregates (RDG-FA) is commonly used to evaluate the radiative properties of soot aerosols composed of nano-spheres due to its analytical character. Despite neglecting electromagnetic coupling within an aggregate, the RDG-FA provides a simple interpretation of angular light-scattering measurements in terms of a structure factor. This factor, in turn, enables the determination of the aggregate's fractal dimension D_f and radius of gyration R_g. The structure factor can be expressed as the Fourier transform of a purely morphological autocorrelation function. Here we employ the discrete dipole approximation and phasor analysis of the internal electric field in an aggregate to study the role of coupling for the specific case of soot particle refractive index. An optical autocorrelation function is defined in terms of an aggregate's phasors rather than simply its physical distribution of material. The new function conveys the effect of the non-uniformity of the internal field distribution, due to coupling, to the angular scattering. A correction term is then introduced explaining why coupling tends to decrease the structure factor inferred in the power-law regime. Such decrease impacts the determination of the fractal dimension from scattering data. Finally, it is shown that the inferred structure factor is mainly affected by a so-called internal trapping effect associated with a large imaginary part of the refractive index.

1. Introduction

The characterization of aerosols, in particular soot, i.e., Black Carbon (BC), has become essential due to its abundance, impact on human health [1,2], and its contribution to atmospheric radiative forcing and related climate impacts [3]. Most soot particles have complex shapes and are frequently considered fractal aggregates as illustrated by the scaling law that makes their virtual generation and study possible [4–6], i.e.,

$$N_m = k_f\left(\frac{R_g}{R_m}\right)^{D_f}. \quad (1)$$

The fractal scaling law of Eq. (1) relates the number N_m of primary nano-spheres, or monomers, in the aggregate to the aggregate size as quantified by its radius of gyration R_g, monomer radius R_m, fractal prefactor k_f, and fractal dimension D_f. The relationship expresses the power-law functionality between particle size and mass or surface.

Angular light scattering has unique characterization capabilities for soot aggregates; it enables the *in-situ* determination of an aggregate'a size and morphology in the visible-wavelength range [7–9] or in the X-ray range with methods such as small angle X-rays scattering (SAXS) [10–12]. Provided the monomers are small, $R_m \ll \lambda$, the Rayleigh scattering law holds, yielding a monomer differential scattering cross section [13,14]:

$$\frac{dC_m^{sca}}{d\Omega} = k^4 R_m^6 F(m). \quad (2)$$

In Eq. (2), $k = 2\pi/\lambda$ is the vacuum wave number, $F(m)$ is the absolute-square of the Lorentz-Lorenz factor $(m^2-1)/(m^2+2)$, the complex-valued refractive index is expressed as $m = n + i\kappa$, and Ω is denotes solid angle.

Assuming that the material is weakly refractive as defined by $m \approx 1$, each monomer is essentially illuminated by only the incident light and not the light scattered by the other monomers, i.e., there is no internal coupling between the monomers. The differential scattering cross section for an aggregate can then be expressed

* Corresponding author.
E-mail address: yon@coria.fr (J. Yon).

https://doi.org/10.1016/j.jqsrt.2022.108451
0022-4073/

by the Rayleigh-Debye-Gans differential scattering cross section:

$$\frac{\mathrm{d}C_{\mathrm{agg}}^{\mathrm{sca}}}{\mathrm{d}\Omega}(\mathbf{q}) = N_{\mathrm{m}}^2 \frac{\mathrm{d}C_{\mathrm{m}}^{\mathrm{sca}}}{\mathrm{d}\Omega} f(\mathbf{q}). \tag{3}$$

In Eq. (3), $f(\mathbf{q})$ is the aggregate structure-factor and $\mathbf{q}$ is the scattering wave vector given by $\mathbf{q} = \mathbf{k}^{\mathrm{inc}} - \mathbf{k}^{\mathrm{sca}}$ where $\mathbf{k}^{\mathrm{inc}}$ and $\mathbf{k}^{\mathrm{sca}}$ are, respectively, the incident and scattering wave vectors. For the forward-scattering direction, $\mathbf{q} \to \mathbf{0}$, any portion of the aggregate is assumed to scatter in phase and $f \to 1$. For larger scattering angles θ, destructive interferences occur across portions of the aggregate, reducing the value of f. This decrease carries information related to the aggregate's R_{g} and D_{f} as described by the RDG-FA theory [7]. Indeed, one can show that f is the Fourier transform of the density autocorrelation function $g(\mathbf{u})$ [15]:

$$f(\mathbf{q}) = \frac{1}{V^2} \int_{\mathbf{u}} g(\mathbf{u}) \exp(i\mathbf{q}\cdot\mathbf{u}) \mathrm{d}\mathbf{u}, \tag{4}$$

where

$$g(\mathbf{u}) = \int_{\mathbf{r}'} \rho(\mathbf{r}' - \mathbf{u}) \rho(\mathbf{r}') \mathrm{d}\mathbf{r}', \tag{5}$$

In Eq. (5), $\rho(\mathbf{r}')$ is the density function expressing whether material is present ($\rho = 1$), or not ($\rho = 0$), at a given position $\mathbf{r}'$. The concept of $g(\mathbf{u})$ is first described in Porod [16] and represents the probability that a point at a distance $\mathbf{u}$ from any given point in the aggregate will itself also be in the aggregate. It is therefore related to the particle size, or volume, and can be used as a morphological descriptor. Unfortunately, an accurate analytical expression for $g(\mathbf{u})$ exists only for simple shapes such as spheres. For this reason, one can find many attempts in the literature to express g, or f, for complex structures like fractal aggregates [7]. Nevertheless, simple and popular approximations exist to interpret the angular scattered intensity in terms of R_{g} in the Guinier regime, and D_{f} in the power-law regime [17].

The RDG-FA approach is popular for the study of soot formation in flames. One can be confident with the assumptions involved in the approximation for X-rays because the refractive index is very close to one. However, the assumptions become much more questionable for visible light as m deviates significantly from one for absorbing materials and internal coupling may not be negligible. For this reason, several studies evaluate the range of validity of the RDG-FA and have shown that the scattering or absorption cross sections can deviate up to 30% compared to more rigorous treatments [18–20]. Some studies were devoted to the improvement of such evaluations by considering more precise determinations of the primary sphere cross sections [21–23]. These deviations have also been investigated for different morphological parameters such as the monomer size distribution [24], the fractal parameters [25–27], the presence of necking and overlapping between neighboring monomers [28], coating [29], and finally, different refractive index values and wavelength [18,19]. This prior work generally reports correction factors, h and A, for the absorption and forward scattering cross sections, respectively. Some studies observe a deviation in the slope of the structure factor in the power-law regime, which could alter the determination of the aggregate fractal dimension from light scattering measurements [18,19,26,30].

More recently, to have a better understanding for the underlying phenomenon, we examine the non-uniformity of the aggregate's internal electric field to understand the origins of the correction terms A and h [31,32]. Indeed, internal coupling can alter the uniformity of the internal field, rendering the Rayleigh approximation invalid. The conclusion is made possible with the help of a mathematical concept called phasor analysis [33] which illustrates the contribution of each element of the aggregate to its overall scattering behavior. The role played by so-called hot-spots of the internal field as well as the decreasing magnitude of light as it crosses an aggregate (trapping) is studied in [31,32]. Also examined is the impact of these effects on the A and h factors, i.e., on forward scattering and absorption. The phasor analysis approach is also applied in an evaluation of backscattering properties of aggregates in [34].

The objective of this work is to extend phasor analysis to the description of the structure factor f, i.e., by investigating the effect of the non-uniform internal electric field on f. We aim to advance the understanding of the mechanisms responsible for deviations of the RDG-FA from the rigorous treatment for backward scattering. The work will provide a physical understanding for previously empirical efforts to determine aggregate size or morphology from backscattering measurements, including the retrieval of number and mass concentration of soot aggregates in smoke plumes using LIDAR [35]. By using a similar approach as Romanov and Yurkin [36], we define an optical autocorrelation function, which is complex-valued in contrast to the real-valued density autocorrelation function. An analytical expression for the structure factor follows, composed of two terms. The first is proportional to the classical expression given in Eq. (4), while the second appears only when internal coupling results in significant field non-uniformity. The findings are illustrated for monomers in point-contact in a diffusion limited cluster-cluster aggregate.

2. Theory

2.1. Optical autocorrelation function

Consider a planar incident wave propagating along the positive x-axis that is linearly polarized along the y-axis in the laboratory reference frame, i.e., $\mathbf{E}^{\mathrm{inc}}(\mathbf{r}) = E_{\mathrm{o}} \exp(ik\hat{\mathbf{x}}\cdot\mathbf{r})\hat{\mathbf{y}}$ where E_{o} is the field magnitude. Emphasis will be placed on the vertical component of the scattered field, i.e., the y-axis direction, which will be denoted by the subscript vv. This is a common experimental configuration (see Fig. 1). In the vertical-vertical polarization configuration, the Volume Integral Equation (VIE) [38] gives:

$$\mathbf{E}_{1,\mathrm{vv},\Psi}^{\mathrm{sca}}(\hat{\mathbf{r}}) = \frac{3k^2}{4\pi} \frac{m^2-1}{m^2+2} E_{\mathrm{o}} \int_V z_{y,\Psi}(\hat{\mathbf{x}}) \exp(i\mathbf{q}\cdot\mathbf{r}') \mathrm{d}\mathbf{r}' \hat{\mathbf{y}}, \tag{6}$$

where Ψ represents a given orientation of the aggregate, $\hat{\mathbf{r}}$ is the scattering direction in the $x-z$ plane, and $z_{y,\Psi}$ is a phasor, which is defined for any point $\mathbf{r}'$ in the aggregate material V. The expression for a phasor for this specific scattering configuration is:

$$z_{y,\Psi}(\hat{\mathbf{x}}) = \frac{m^2+2}{3E_0} E_{y,\Psi}^{\mathrm{int}}(\mathbf{r}') \exp(-ik\mathbf{x}'). \tag{7}$$

where $E_{y,\Psi}^{\mathrm{int}}$ is the internal electric field in a volume element $\mathrm{d}\mathbf{r}'$ at $\mathbf{r}'$ in V. Note that, the phasors are only defined inside the aggregate as the integral in Eq. (6) runs over V. This field can be found numerically via the DDA as implemented with the DDSCAT software of Draine and Flatau [39] for a given aggregate orientation Ψ. Note that, $z_{y,\Psi} = 1$ at any point in the aggregate if the RDG-FA criteria are fulfilled. For a more detailed description of the mathematical development leading to Eq. (6), the reader may refer to [31,32]. Note, however, that these works are focused on the forward scattering while the main interest here is the angular dependence of the scattered intensity by rotating the scattering direction $\hat{\mathbf{r}}$ in the $x-z$ plane by an angle θ. Given Eq. (6), the differential scattering cross section for vertical-vertical polarization is:

$$\frac{\mathrm{d}C_{\mathrm{vv},\Psi}^{\mathrm{sca}}}{\mathrm{d}\Omega}(\hat{\mathbf{r}}) = \left(\frac{3k^2}{4\pi}\right)^2 F(m) \left| \int_V z_{y,\Psi}(\hat{\mathbf{x}}') \exp(i\mathbf{q}\cdot\mathbf{r}') \mathrm{d}\mathbf{r}' \right|^2 \tag{8}$$

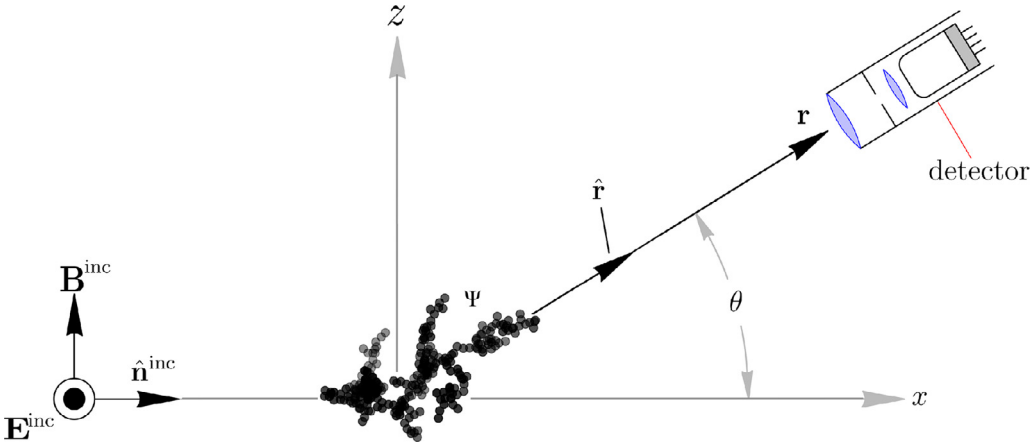

Fig. 1. Scattering configuration, Ψ is the orientation of the aggregate as defined in Section 19 of [37].

Expanding the absolute-square in Eq. (8) allows one to write:

$$\frac{\mathrm{d}C^{\mathrm{sca}}_{\mathrm{vv},\Psi}}{\mathrm{d}\Omega}(\hat{\mathbf{r}}) = \left(\frac{3k^2}{4\pi}\right)^2 F(m) \int_V\int_V z_{y,\Psi}(\mathbf{r}')z^*_{y,\Psi}(\mathbf{r}'') \exp[i\mathbf{q}\cdot(\mathbf{r}'-\mathbf{r}'')]\mathrm{d}\mathbf{r}''\mathrm{d}\mathbf{r}'. \tag{9}$$

Then, a change of variables, $\mathbf{u} = \mathbf{r}' - \mathbf{r}''$ and $\mathrm{d}\mathbf{u} = \mathrm{d}\mathbf{r}'$ may be done, giving a new expression for the differential cross section:

$$\frac{\mathrm{d}C^{\mathrm{sca}}_{\mathrm{vv},\Psi}}{\mathrm{d}\Omega}(\hat{\mathbf{r}}) = \left(\frac{3k^2}{4\pi}\right)^2 F(m) \int_{\mathbb{R}^3} g^{\mathrm{opt}}_{\Psi}(\mathbf{u}) \exp(i\mathbf{q}\cdot\mathbf{u})\mathrm{d}\mathbf{u} \tag{10}$$

with g^{opt}_{Ψ} representing the so-called optical autocorrelation function defined as:

$$g^{\mathrm{opt}}_{\Psi}(\mathbf{u}) = \int_V z_{y,\Psi}(\mathbf{r}''+\mathbf{u})z^*_{y,\Psi}(\mathbf{r}'')\mathrm{d}\mathbf{r}''. \tag{11}$$

Note that now, the differential scattering cross section for vertical-vertical polarization is given in terms of the Fourier transform of g^{opt}_{Ψ} whose accuracy depends on that of the numerical solution of the internal electric field used for the determination of the phasor. Readers interested in evaluating the autocorrelation function based on internal fields for unpolarized light can refer to the article [36]. The function g^{opt}_{Ψ} becomes identical to the density autocorrelation function, g of Eq. (5), only if the phasors equal 1, i.e., when RDG-FA hypotheses are fulfilled. When non-uniformity of the internal electric field is present, which is a violation of the RDG-FA assumptions, g^{opt}_{Ψ} returns complex numbers even if its Fourier transform still yields the real-valued differential cross section, i.e., Eq. (10). Next, we examine the properties of the optical autocorrelation function, g^{opt}_{Ψ}.

2.2. Properties of the optical autocorrelation function

We first evaluate g^{opt}_{Ψ} at the origin, where the result is proportional to the aggregate's physical volume. The proportionality coefficient is found to be $\left|\overline{z_{y,\Psi}}\right|^2$, which has been identified as a proxy for the correction factor $h_{\mathrm{v}}(\Psi)$ of [31] that brings the RDG-FA theory absorption cross section into agreement with the true value. Specifically,

$$g(\mathbf{u}=\mathbf{0}) = \overline{\left|z_{y,\Psi}\right|^2}V \approx h_{\mathrm{v}}(\Psi)V \quad \text{and}$$
$$\int_{\mathbb{R}^3} g^{\mathrm{opt}}_{\Psi}(\mathbf{u})\mathrm{d}\mathbf{u} = \left|\overline{z_{y,\Psi}}\right|^2 V^2 = A_{\mathrm{vv}}(\Psi)V^2. \tag{12}$$

It can be shown that integrating the optical autocorrelation function is proportional to the squared aggregate's volume and to $\left|\overline{z_{y,\Psi}}\right|^2$ which is shown to be $A_{\mathrm{vv}}(\Psi)$, i.e., the forward-scattering cross section RDG-FA correction in [31]. Thus, in addition to the purely morphological description of the particle, the optical autocorrelation function conveys information about intrinsic optical properties that explain the deviation from RDG-FA theory.

The phasors are complex numbers, $z_{y,\Psi} = a + ib$, and so, the optical autocorrelation function can be decomposed into real and imaginary parts:

$$g^{\mathrm{opt}}_{\Psi}(\mathbf{u}) = g_{\mathrm{re},\Psi}(\mathbf{u}) + ig_{\mathrm{im},\Psi}(\mathbf{u}). \tag{13}$$

where

$$g_{\mathrm{re},\Psi}(\mathbf{u}) = \int_V a(\mathbf{r}''+\mathbf{u})a(\mathbf{r}'')\mathrm{d}\mathbf{r}'' + \int_V b(\mathbf{r}''+\mathbf{u})b(\mathbf{r}'')\mathrm{d}\mathbf{r}'',$$
$$g_{\mathrm{im},\Psi}(\mathbf{u}) = \int_V a(\mathbf{r}'')b(\mathbf{r}''+\mathbf{u})\mathrm{d}\mathbf{r}'' - \int_V a(\mathbf{r}''+\mathbf{u})b(\mathbf{r}'')\mathrm{d}\mathbf{r}''. \tag{14}$$

First, consider the case when $m \to 1$, the RDG-FA case. Here, there is no internal coupling, as would be the case with X-rays measurements, and $z_{y,\Psi} \to 1$, i.e., $a = 1$ and $b = 0$ so $g_{\mathrm{im},\Psi}(\mathbf{u})$ vanishes and $g_{\mathrm{re},\Psi}(\mathbf{u}) = g(\mathbf{u})$. In that case, $g_{\mathrm{re},\Psi}(\mathbf{u})$ conveys only the aggregate's morphological description and the classical RDG-FA treatment is valid.

When $m > 1$ and thus $z_{y,\Psi} \neq 1$, one can show based on Eq. (14) and an appropriate change of variables that $g_{\mathrm{re},\Psi}(\mathbf{u})$ is an even function. Conversely, because $g_{\mathrm{im},\Psi}(\mathbf{u})$ depends on the cross product of the real and imaginary parts of the phasor, one can see that $g_{\mathrm{im},\Psi}(\mathbf{u}=\mathbf{0}) = 0$ and $g_{\mathrm{im},\Psi}(-\mathbf{u}) = g_{\mathrm{im},\Psi}(\mathbf{u})$, and so, is an odd function. Because the phasors depend on the aggregate orientation, one can evaluate an orientation averaged optical autocorrelation function, denoted by g^{opt} or

$$g^{\mathrm{opt}}(\mathbf{u}) = \langle g^{\mathrm{opt}}_{\Psi}(\mathbf{u})\rangle_{\Psi} = g_{\mathrm{re}}(\mathbf{u}) + ig_{\mathrm{im}}(\mathbf{u}), \tag{15}$$

with $g_{\mathrm{re}}(\mathbf{u}) = \langle g_{\mathrm{re},\Psi}(\mathbf{u})\rangle_{\Psi}$ and $g_{\mathrm{im}}(\mathbf{u}) = \langle g_{\mathrm{im},\Psi}(\mathbf{u})\rangle_{\Psi}$.

2.3. Internal coupling and the structure factor

As mentioned above, the correction factors $A = \langle A_{\mathrm{vv}}\rangle_{\psi}$ to the RDG-FA forward scattering are discussed in [32]. The objective here is to focus on the specific impact of internal coupling on the structure factor f, as this function is used with the correction factor in the RDG-FA theory, i.e.,

$$\frac{\mathrm{d}C^{\mathrm{sca}}_{\mathrm{agg,vv},\Psi}}{\mathrm{d}\Omega}(\mathbf{q}) = A_{\mathrm{vv}}(\Psi)N^2_{\mathrm{m}}\frac{\mathrm{d}C^{\mathrm{sca}}_{\mathrm{m,vv}}}{\mathrm{d}\Omega}f^{\mathrm{IC}}_{\Psi}(\mathbf{q}), \tag{16}$$

where the superscript IC denotes the presence of internal coupling. Similarly, when dealing with orientation-averaged aggregates:

$$\frac{\mathrm{d}C^{\mathrm{sca}}_{\mathrm{agg,vv}}}{\mathrm{d}\Omega}(\mathbf{q}) = AN^2_{\mathrm{m}}\frac{\mathrm{d}C^{\mathrm{sca}}_{\mathrm{m,vv}}}{\mathrm{d}\Omega}f^{\mathrm{IC}}(\mathbf{q}). \tag{17}$$

By comparing Eq. (10) and Eq. (16) one finds that for fixed-orientation aggregates (Ψ), we have:

$$f_{\Psi}^{\mathrm{IC}}(\mathbf{q}) = \frac{\int_{\mathbb{R}^3} g_{\Psi}^{\mathrm{opt}}(\mathbf{u}) \exp(i\mathbf{q}\cdot\mathbf{u})\mathrm{d}\mathbf{u}}{\int_{\mathbb{R}^3} g_{\Psi}^{\mathrm{opt}}(\mathbf{u})\mathrm{d}\mathbf{u}} = \frac{1}{A_{\mathrm{vv}}(\Psi)V^2}\int_{\mathbb{R}^3} g_{\Psi}^{\mathrm{opt}}(\mathbf{u}) \exp(i\mathbf{q}\cdot\mathbf{u})\mathrm{d}\mathbf{u}. \tag{18}$$

Similarly, for orientation averaged aggregates via Eq. (17) we have:

$$f^{\mathrm{IC}}(\mathbf{q}) = \frac{\int_{\mathbb{R}^3} g^{\mathrm{opt}}(\mathbf{u}) \exp(i\mathbf{q}\cdot\mathbf{u})\mathrm{d}\mathbf{u}}{\int_{\mathbb{R}^3} g^{\mathrm{opt}}(\mathbf{u})\mathrm{d}\mathbf{u}} = \frac{1}{AV^2}\int_{\mathbb{R}^3} g^{\mathrm{opt}}(\mathbf{u}) \exp(i\mathbf{q}\cdot\mathbf{u})\mathrm{d}\mathbf{u}, \tag{19}$$

By separating Eqs. (18–19) into real and imaginary parts, one can show that the structure factor accounting for internal coupling can finally be seen as the difference of two terms, expressed in the following only for the orientation-averaged aggregate case as:

$$f^{\mathrm{IC}}(\mathbf{q}) = f_1(\mathbf{q}) - f_2(\mathbf{q}), \tag{20}$$

where $f_1(\mathbf{q})$ is:

$$f_1(\mathbf{q}) = \frac{\int_{\mathbb{R}^3} g_{\mathrm{re}}(\mathbf{u}) \cos(\mathbf{q}\cdot\mathbf{u})\mathrm{d}\mathbf{u}}{\int_{\mathbb{R}^3} g_{\mathrm{re}}(\mathbf{u})\mathrm{d}\mathbf{u}}. \tag{21}$$

Importantly, note that the denominator in Eq. (21) only depends on the real part of the optical autocorrelation function as $\int_{\mathbb{R}^3} g_{\mathrm{im}}(\mathbf{u})\mathrm{d}\mathbf{u} = 0$.

For $m \to 1$, $g_{\mathrm{re}}(\mathbf{u}) \to g(\mathbf{u})$. Moreover, as the aggregates do not present any favoured direction, when the autocorrelation functions are averaged over all the considered aggregate orientations an isotropic function is obtained $g(\mathbf{u}) = g(u)$, and the classical formula for the determination of the structure factor [15] is found:

$$f_1(q) \to f(q) = \frac{4\pi}{V^2}\int_0^{\infty} g(u)\frac{\sin(qu)}{qu}u^2\mathrm{d}u. \tag{22}$$

For $m > 1$, meaning when internal coupling is significant, the fact that incident light is vertically polarized can violate the isotropic assumption of this equation for $g_{\mathrm{re}}(\mathbf{u})$. This will be discussed in Section 4.1. Meanwhile, the second part of Eq. (20), $f_2(\mathbf{q})$, is given by:

$$f_2(\mathbf{q}) = \frac{\int_{\mathbb{R}^3} g_{\mathrm{im}}(\mathbf{u}) \sin(\mathbf{q}\cdot\mathbf{u})\mathrm{d}\mathbf{u}}{\int_{\mathbb{R}^3} g_{\mathrm{re}}(\mathbf{u})\mathrm{d}\mathbf{u}}. \tag{23}$$

When $m = 1$, there is no internal coupling, and therefore, $g_{\mathrm{im}}(\mathbf{u})$ and $f_2(\mathbf{q})$ are zero. However, when $m > 1$, $g_{\mathrm{im}}(\mathbf{u})$ differs from zero. As the sine function is an odd function, the integral of their product is non-zero. The following will study how f_1 deviates from the purely morphological autocorrelation function g, examine the new term f_2, and evaluate their impact on the structure factor.

3. Numerical study

We will focus on Diffusion Limited Cluster Aggregates (DLCA) [40] exhibiting a clear fractal character. Most of the results presented here are based on a single aggregate taken from Sorensen et al. [19] having $N_{\mathrm{m}} = 284$ monomers, and representative of a $D_{\mathrm{f}} = 1.78 \pm 0.04$ aggregate with $k_{\mathrm{f}} = 1.35 \pm 0.10$ and averaged over 500 orientations isotropicaly distributed. For Fig. 9, in order to avoid specific morphological dependence and extend our analysis, we make use of the ergodicity theorem to abandon orientation averaging, and rather, average over 540 different DLCA aggregates taken from Yon et al. [41] with $N_{\mathrm{m}} \in [10, 300]$, $D_{\mathrm{f}} \approx 1.78$ and $k_{\mathrm{f}} \approx 1.4$, and where each aggregate has an arbitrary fixed orientation. However, in each cases, the monomer radius is fixed at 15nm.

The wavelengh is fixed at 266nm in the study. For the material refractive index, the real part ranges from 1.1 to 1.9 and the imaginary part from 0.01 to 0.8. However, in the first part of the study, in order to illustrate the phenomenon, the index is fixed at $m = 1.1 + i0.8$ corresponding to soot material at this wavelength.

The internal electric fields are computed with DDSCAT which numerically solves the VIE [42]. In this method, the aggregates volume V is discretized on a cubic lattice of lattice spacing d to form volume elements $\Delta V = d \times d \times d$. The accuracy of the solution depends on the fineness of this lattice, i.e., the value of d, as compared to λ and has to fulfill the condition $|m|kd < 0.5$. To satisfy this condition, 110 dipoles per monomer have been considered here, which is shown to be sufficient as basic considerations in [43] suggest 34 for point-contact monomers is sufficient.

4. Results

4.1. Autocorrelation function

The real and imaginary parts of the averaged optical autocorrelation function are reported in Fig. 2, respectively, in Fig. 2(a) and Fig. 2(c) where one sees the behavior in the $x - z$ plane. The colors correspond to amplitudes in log-scale as the functions rapidly decrease as illustrated in linear-scale along the x-axis direction in plots (b) and (d).

Plots Fig. 2(a) and Fig. 2(b) clearly illustrate the central symmetry of $g_{\mathrm{re}}(u_x, u_y = 0, u_z)$ which is consistent with the property $g_{\mathrm{re}}(-\mathbf{u}) = g_{\mathrm{re}}(\mathbf{u})$. Moreover, as in g, g_{re} seems to show an isotropic character in this plane $g_{\mathrm{re}}(\mathbf{u}) \approx g_{\mathrm{re}}(u)$. Conversely, plots Fig. 2(c) and Fig. 2(d) illustrate the asymmetric character of g_{im}. One can see that the amplitude of g_{re} and g_{im} decrease rapidly away from $\mathbf{u} = \mathbf{0}$. Nevertheless, $g_{\mathrm{re}}(\mathbf{0})$ is a maximum whereas $g_{\mathrm{im}}(\mathbf{0})$ is zero.

We show in [32] that the amplitude of the internal electric field decreases along the axis of incident light propagation and the phase increases in this direction. This effect is attributed to a so-called internal trapping. Because the real part of the optical autocorrelation function $g_{\mathrm{re}}(\mathbf{u})$ depends on the internal electric field, one may wonder if this preferred direction could break the isotropy found in the conventional autocorrelation function, g. Work by Heinson et al. [44] introduces a method to evaluate the anisotropy of an aggregate based on the ratio between the maximum and minimum values of the eigenvalues of the aggregates mass inertia-matrix. Since the gyration radius can also be determined from the autocorrelation function (Appendix A of [7]), we can define a gyration radius for each plane as illustrated for the specific $x - z$ plane here:

$$R_{\mathrm{g,xy}} = \frac{\int_0^{\infty} u^3 g_{\mathrm{re}}(u_{\mathrm{x}}, u_{\mathrm{y}}, u_{\mathrm{z}} = 0)\,\mathrm{d}u}{2\int_0^{\infty} u\, g_{\mathrm{re}}(u_{\mathrm{x}}, u_{\mathrm{y}}, u_{\mathrm{z}} = 0)\,\mathrm{d}u}. \tag{24}$$

Thus the anisotropy of g_{re} can be illustrated by a variability of the gyration radius in each considered plane.

For the range of refractive indices considered, $n \in [1.1 - 1.9]$ and $\kappa \in [0.01 - 0.8]$, which are sufficient to cover the range of soot indices, and for the aggregate considered ($N_{\mathrm{m}} = 284$), the relative deviation from one plane to another never exceeds 1%. This empirical observation allows us to say that real part of the autocorrelation function after averaging over orientations is approximately isotropic for similar objects and refractive indices.

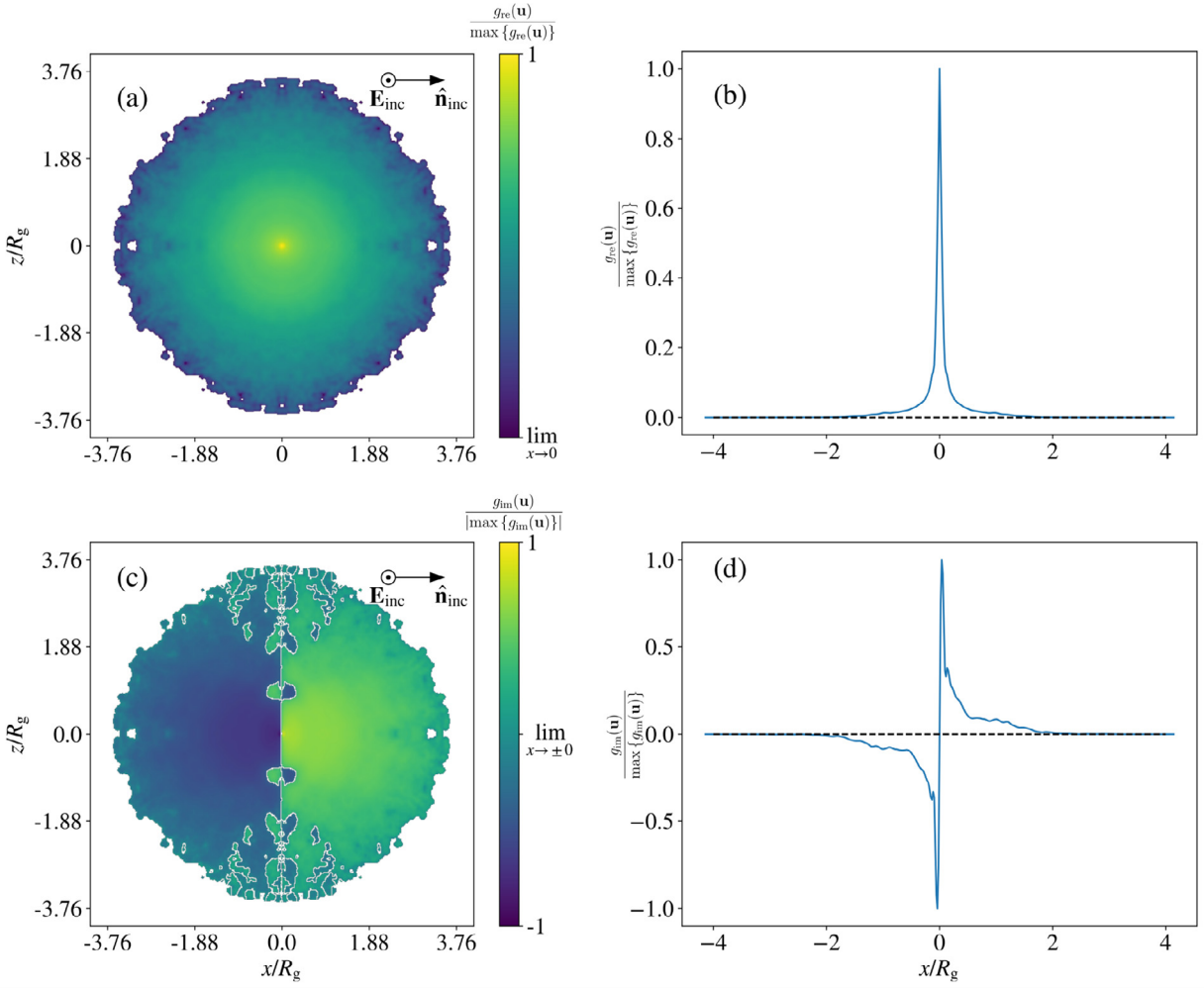

Fig. 2. Section of the optical autocorrelation function averaged over 500 orientations of the aggregate ($N_{\rm m} = 284$, $R_{\rm m} = 15\,{\rm nm}$) in the $x - z$ plane for $m = 1.1 + i0.8$ at $\lambda = 266\,{\rm nm}$. The top row reports the real part $g_{\rm re}$ while the bottom row reports the imaginary part $g_{\rm im}$.

Nevertheless, in the following, no hypothesis of isotropy will be used for the determination of the structure factors f_1 and f_2. Instead, the 3D description of the pairwise autocorrelation [see Eq. (21) and Eq. (23)] will be used.

The fact that $g_{\rm re}$ is approximately isotropic allows us to see the effect of the non-uniformity of the internal electric field directly by comparing $g(u)$ and $g_{\rm re}(u)$ which are averaged over all the directions of $\mathbf{u}$ in $\mathbb{R}^3$. This is shown in Fig. 3 which reports in black dashed line the conventional, i.e., purely morphological, autocorrelation function $g(u)$ for the same aggregate as in Fig. 2 after averaging over all orientations. The x-coordinate is normalized by the aggregate gyration diameter whereas the y-axis is normalized by the aggregate volume. This normalization ensures a convergence to 1 for the function as $u \to 0$ and becomes zero when u approaches $\approx 1.5D_{\rm g}$. Its integral corresponds to the aggregate volume. This function exhibits a power-law dependence for $0.05 < u/D_g < 0.4$ with a slope of $D_{\rm f} - 3$, which is typical for fractal aggregates. For lower u, the function is dominated by the monomer self-interaction effect and for larger u it is affected by the cutoff function, see [41]. The $g_{\rm re}(u)$ function is reported by the blue curve, which is clearly different from the purely morphological g, even if it is approximately isotropic. This deviation is due to the spatial departure of the phasor from 1 caused by internal coupling. Since the spatial extent of the aggregate is obviously not affected by the non-uniformity of the electric field, this function naturally ends for the same value of u. On the other hand, this function is affected for smaller u. As shown above, the integration of that function, which is shown by the colored shaded region, corresponds to the forward-scattering correction A multiplied by the aggregate volume, V. Here, $m = 1.1 + i0.8$ for $\lambda = 266nm$ and $A \approx 0.61$, which implies that the function intercepts the y-axis at a value less than 1. Also discussed above is that $g_{\rm re}(0)/V \approx h$, where h is the absorption cross section correction for RDG. This correction is of the same order as A, i.e., $h/A \approx 1.07$, see Argentin et al. [31]. It is notable that a simple multiplication of $g(u)$ by A, which is represented by red circles in the plot, produces a very good approximation for $g_{\rm re}(u)$. This suggests that the structure factor is nearly unaffected by internal coupling as long as A is taken into account, which would be a good approximation if $g_{\rm im}$ is zero. Due to its non isotropic nature, $g_{\rm im}$ cannot be represented in Fig 3. The next section, however, will illustrate the impact of $g_{\rm im}$ on the structure factor.

4.2. Structure factor

The structure factor can be obtained by normalizing to 1 the differential scattering cross section for the vertical-vertical polarization case calculated by DDSCAT. When the result called "DDSCAT" in blue dash-dot line in Fig. 4, is compared with our optical structure factor $f^{\rm IC}$ in red circles, the two are superimposed. This proves that our mathematical development and numerical post-processing of the internal electric field of the aggregate calculated by DDSCAT are correct. The purely morphological

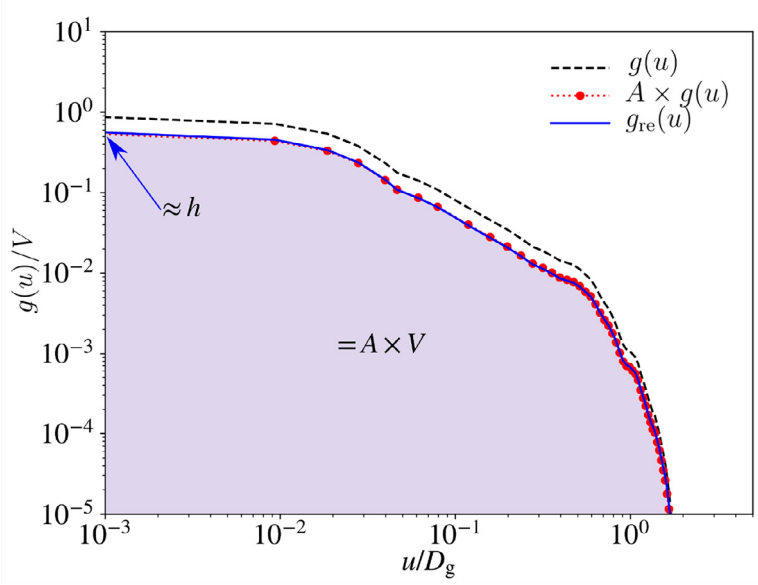

Fig. 3. Comparison of the conventional autocorrelation function (black dashed line) with that corrected by the forward scattering correction term A (red circle marker) and the real part of the pair correlation function following orientation averaging (blue solid line). Shown is the same aggregate as Fig. 2.

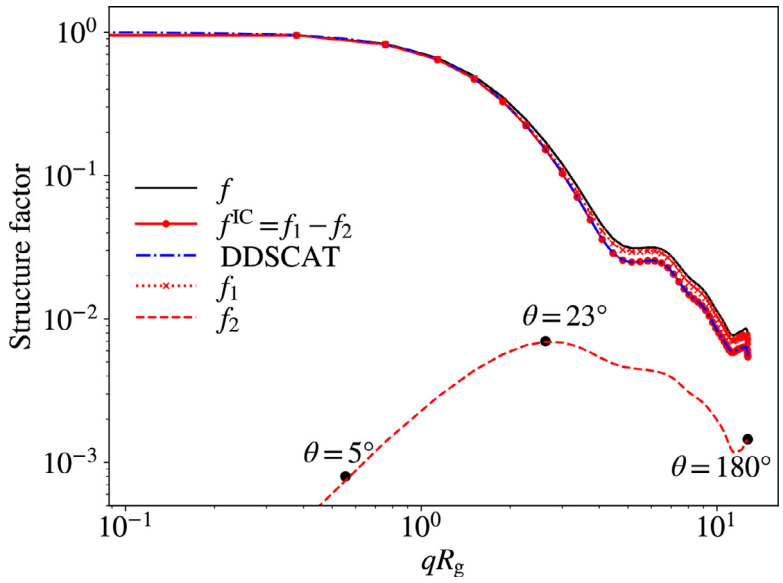

Fig. 4. Comparison of different structure factors calculated for a DLCA aggregate composed of 284 monomers with a monomer radius $R_{\mathrm{m}} = 15\,\mathrm{nm}$ for $m = 1.1 + i0.8$ at $\lambda = 266\,\mathrm{nm}$. Respectively, the morphological function f (black solid line), that generated via phasors f^{IC} (in red circle marker), that of f_1 (red "x" marker), f_2 (red dashed line), and that generated by DDSCAT.

structure factor f computed by considering the phasor equal to $z_y = 1$ is reported in black line. One can see that it decreases more rapidly when internal coupling is considered. Consequently, internal coupling tends to overestimate the fractal dimension up to 10% as reported by Yon et al. [18]. Fig. 4 also shows the contribution of f_1 and f_2 [see Eqs. (21 and 23)]. The log-log plot renders f_1 and f similar, yet they do not fully agree. The departure begins to increase beyond the Guinier regime, i.e., for $qR_{\mathrm{g}} > 1$, and can reach up to 10% when $\theta = 180°$. Similarly, f_2 contributes at larger q values. Thus, the Guinier regime, and therefore the determination of R_{g} from measurements, are in the end unaltered by internal coupling. When the structure factor is evaluated with the Guinier equation, i.e., $f(q) = \exp(-q^2 R_{\mathrm{g}}^2/3)$, the difference between the corresponding R_{g} values based on f^{IC} or f never exceed 1% (this was expected due to the quasi isotropy of g_{re} for the present study). For the behavior of f_2 at larger qR_{g} values, one can see its growth to $\theta \approx 23°$ depending on the morphology of the aggregate, which corresponds to a qR_{g} value close to the beginning of the power-law regime. After reaching this maximum, f_2 begins to decrease. This particular behavior will be discussed below where it is finally shown to have a more important impact than f_1 on the effective structure factor derived in the power-law regime.

4.3. Interpretation of the angular dependence of the structure factor

As shown in Eq. (21) and Eq. (23), the components f_1 and f_2 result, respectively, from the cosine and sine modulation of the real and imaginary part of the optical autocorrelation function. As suggested by Berg et al. [33], this modulation can be illustrated graphically to achieve a phenomenological understanding. The dif-

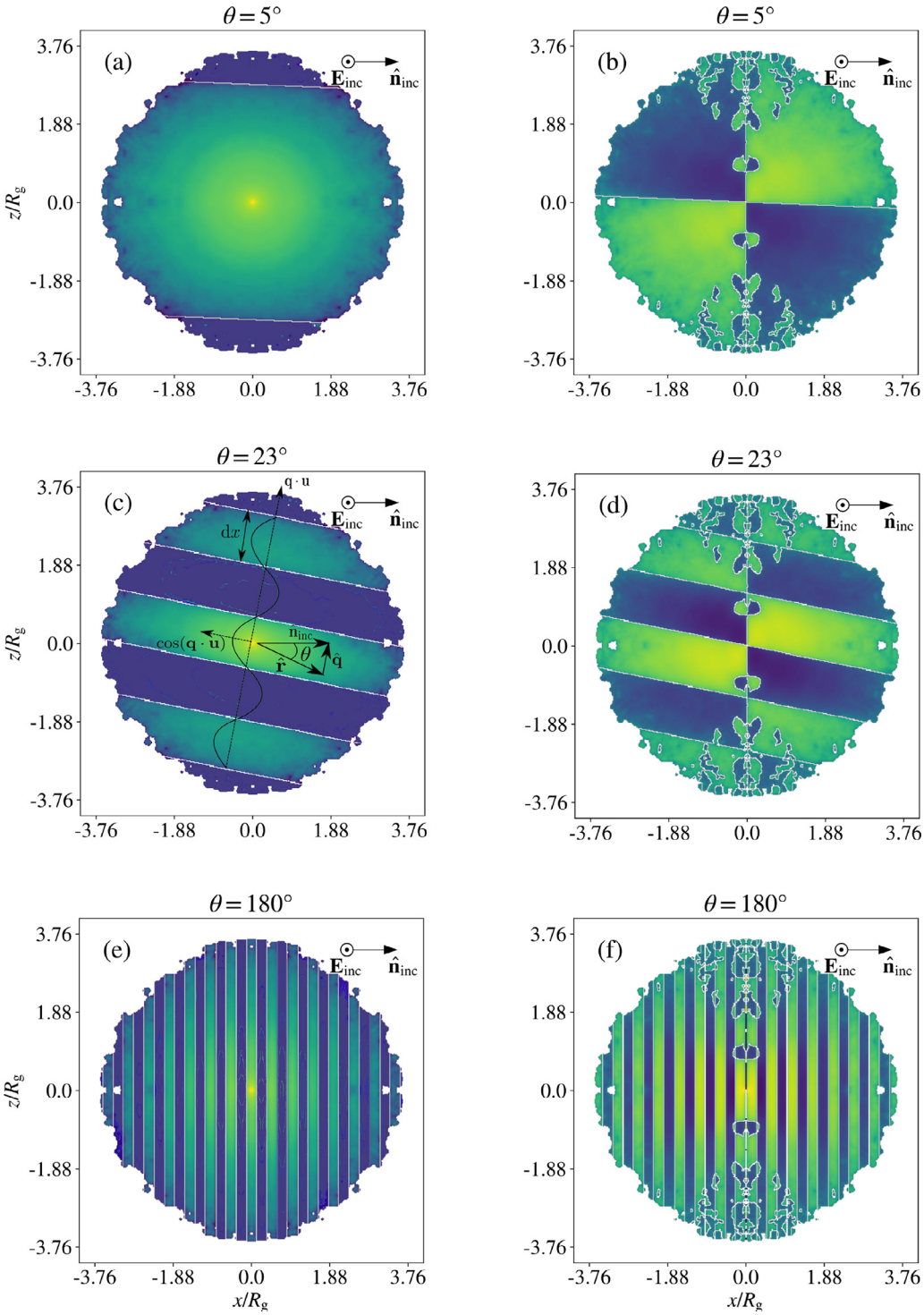

Fig. 5. Section of $g_{\mathrm{re}}(\mathbf{u})\cos(\mathbf{q}\cdot\mathbf{u})$ in the plots (a), (c), (e) and $g_{\mathrm{im}}(\mathbf{u})\sin(\mathbf{q}\cdot\mathbf{u})$ in the plots (b), (d), (f) for three different scattering angles θ for $m = 1.1 + i0.8$ at $\lambda = 266$ nm.

ference here is that the slicing approach is applied to the autocorrelation components and not directly to the physical material. Fig. 5 presents, in the left column, the contribution of f_1 while the right shows f_2. The three rows corresponds to near-forward scattering at $\theta = 5°$, side scattering at $\theta = 23°$, and backscattering at $\theta = 180°$; these are the angles corresponding to the labled symbols in Fig. 4.

The illustrations in Fig. 5 are restricted to the $x - z$ plane as a function of θ. The slices are caused by the cosine and sine modulations. Increasing the scattering angle θ, and thus q, increases the number of slices spanning the autocorrelation pattern since the thickness dx of the slices is inversely proportional to q [7,33]. Also, increasing q rotates the modulation pattern in a clockwise direction until it becomes orthogonal to the incident light direction for $\theta = 180°$. As the slices are caused by the cosine, some of them will be negative (blue), which reduces the total contribution to f_1. Moreover, as almost all the contribution is contained in the center, the thinner the slices, the smaller the contribution as the cosine weight is not always 1. At small scattering angles, cosine tends to 1 and the structure factor f_1 thus tends to 1 as

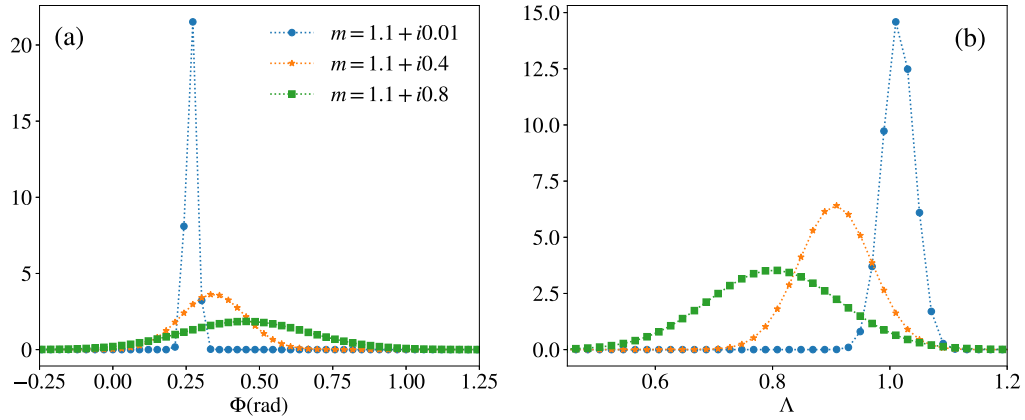

Fig. 6. Probability density function of the phasor-phase (a) and amplitude (b) for three refractive indices, $m = 1.1 + i0.01$, $m = 1.1 + i0.4$, and $m = 1.1 + i0.8$.

well, see Eq. (21). Similarly, for $\theta \to 0^\circ$, the odd f_2 is divided into two regions of opposite sign orthogonal to the incident-light direction. The integration of this modulated domain is close to zero, i.e., the green regions compensate the blue regions. This compensation does not hold when the scattering angle increases as illustrated for $\theta = 23^\circ$ in Fig. 5(d), where f_2 is maximum. Indeed, as f_2 starts at zero for $\theta = 0^\circ$, when the antisymmetry of g_{im} [carried by the $y - z$ plane at $x = 0$, see Fig. 2(c)] is broken due to the slices, it can only grow, i.e. the blue parts no longer compensate for the green parts $f_2 > 0$ [see Fig. 5(b,d,e)]. However, as can be seen in Figure 1(d), most of the contribution of g_{im} is carried by the center $\mathbf{u} \approx \mathbf{0}$. Therefore, the evolution of f_2 depends on how its center is sliced, i.e. the thickness of the green part and the blue part located near $\mathbf{u} \approx \mathbf{0}$. Initially, f_2 increases due to the breaking of the asymmetry. Then, as the slices become thinner, the total contribution becomes progressively more divided between the blue (negative) and green (positive) parts. This leads to a decrease in f_2 which is therefore linked to a geometric effect of the slices on $g_{\text{im}}(\mathbf{u} \approx \mathbf{0})$.

4.4. Internal trapping effect

The previous sections have shown that non-uniformity of the internal electric field has an impact on the structure factor in particular by introducing a term induced by the complex nature of the optical autocorrelation function. In our prior work, it is shown that such non-uniformity can take two forms: hot spots at the vicinity of the contact between monomers and a decrease of the internal electric field accompanied by an increase of the phase shift in the direction of the light propagation caused by so-called internal trapping [31,32]. Here, we focus on the role of this internal trapping on the optical structure factor's deviation from the purely morphological function. This is done by varying the imaginary part of the refractive index.

Fig. 6 (a) shows the probability density function (PDF) of the phasor amplitude Λ after averaging over aggregate orientations. Recall that a phasor is proportional to the internal electric field. Plot (b) reports the same analysis for the phase Φ of the phasor. The three curves correspond to the refractive indices $m = 1.1 + i0.01$, $m = 1.1 + i0.4$, and $m = 1.1 + i0.8$ (chosen arbitrarily in order to vary κ). Yet, note that the index $m = 1.1 + i0.8$ is not far from a graphitic soot index for this wavelength [19]. The dispersion seen in the PDF is a good indicator of internal trapping and is clearly correlated with the increase of the imaginary part of the refractive index. Some elements of the aggregate correspond to amplitudes Λ larger than 1. This is explained by the hot-spots whereas low amplitudes and large phase shifts are generally attributed to the trapping effect.

It is interesting to analytically express the dependence of the two components of the structure factor f_1 and f_2 in terms of the phasor magnitude and phase dispersion. This is simply done by expressing the phasor by its Euler expression $z_y = \Lambda \exp(i\Phi)$ in Eqs. (21, 23):

$$f_1(\mathbf{q}) = \frac{1}{AV^2}\int_{\mathbb{R}^3}\int_V \Lambda(\mathbf{r}''+\mathbf{u})\Lambda(\mathbf{r}'')\cos\left[\Phi(\mathbf{r}''+\mathbf{u})-\Phi(\mathbf{r}'')\right]\cos(i\mathbf{q}\cdot\mathbf{u})\,\mathrm{d}\mathbf{r}''\mathrm{d}\mathbf{u},$$
$$f_2(\mathbf{q}) = \frac{1}{AV^2}\int_{\mathbb{R}^3}\int_V \Lambda(\mathbf{r}''+\mathbf{u})\Lambda(\mathbf{r}'')\sin\left[\Phi(\mathbf{r}''+\mathbf{u})-\Phi(\mathbf{r}'')\right]\sin(i\mathbf{q}\cdot\mathbf{u})\,\mathrm{d}\mathbf{r}''\mathrm{d}\mathbf{u}. \quad (25)$$

This alternative expression is interesting as it highlights the role played by the phase dispersion of the internal electric field. Indeed, without the dispersion of Φ, the cosine in the expression of f_1 is 1 and the sine in the expression of f_2 is zero; this explains the absence of the latter component of the structure factor in RDG-FA theory. The amplitude Λ will essentially affect the magnitude of the scattering cross sections but this is partially neutralized by the correction factor A in the denominator in Eq. (25), which causes the structure factor to tend toward 1 when scattering angle tends toward 0° according to Eqs. (16–17). Based on these equations, the greater the dispersion in phase Φ, the more the optical structure factor will deviate from f.

Fig. 7 (a) confirms our interpretations above where the structure factors are shown for four different refractive indices $m = 1$, $m = 1.1 + i0.01$, $m = 1.1 + i0.4$, and $m = 1.1 + i0.8$. The deviations from the $m = 1$ case are clearly related to the imaginary part of the refractive index. Fig. 7(b) presents the ratio f^{IC}/f to quantify the deviation from the structure factor f. This plot confirms that the trapping effect causes a deviation of the optical structure factor that becomes enhanced for $qR_g \geq 1$, thus explaining why the gyration diameter determination by angular light scattering experiments is largely unaffected. Conversely, the departure in the power-law regime is significant. Indeed, for the refractive index $m = 1.1 + i0.8$, the relative deviation of the structure factor in backscattering reaches 25%. It is also interesting to observe bumps, suggesting that internal coupling is sensitive to the morphological features of the aggregate as such bumps precisely correlate with f, see Fig. 7(a).

Fig. 8 reports the ratio f_2/f for different refractive indices. The general pattern appears to be a rapid growth followed by an asymptotic trend. The three previously studied refractive indices $m = 1.1 + i0.01$, $m = 1.1 + i0.4$, and $m = 1.1 + i0.8$ cause a maximum deviation of 2%, 10% and 20% at $\theta = 180^\circ$, respectively. This confirms the fact that the deviation between f^{IC} and f is mostly driven by f_2. In this curve, the different real parts of the refractive index $\text{Re}\{m\} = n$ reported in Table 1 are considered as well.

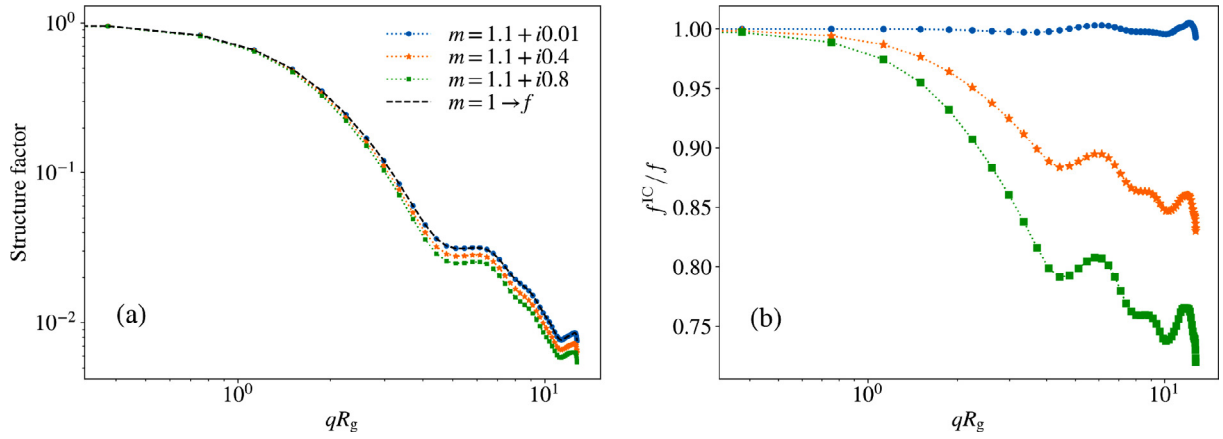

Fig. 7. (a) The structure factor for refractive indices, $m = 1.1 + i0.01$ (circle marker), $m = 1.1 + i0.4$ (star marker), $m = 1.1 + i0.8$ (square marker), and $m = 1$ (black dashed line). In (b) is shown the ratio between the exact structure factor f^{IC} and f, the one considered in RDG-FA with $m = 1$.

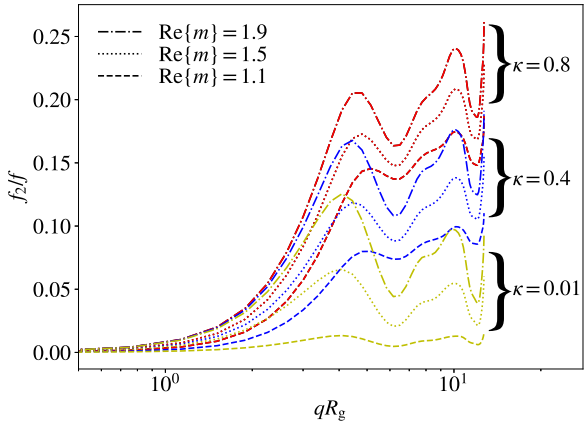

Fig. 8. Ratio between f_2 and f for several indices. For the three κ, the dashed lines correspond to refractive indices with $\mathrm{Re}\{m\} = 1.1$, the dot lines with $\mathrm{Re}\{m\} = 1.5$, and the dashed-dot lines with $\mathrm{Re}\{m\} = 1.9$ (see Table 1).

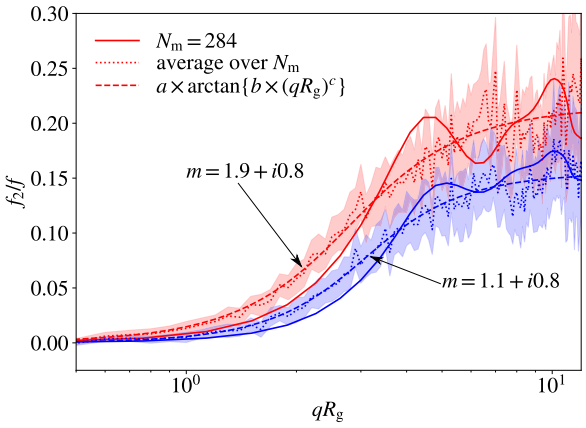

Fig. 9. Ratio between f_2 and f for $m = 1.9 + i0.8$ and $m = 1.1 + i0.8$ at $\lambda = 266$ nm. The individual behavior is reported in plain curves. The average result based on many DLCA aggregates is reported in dot lines and its fit in dash lines. The color shaded areas indicate the 95% confidence interval.

Table 1
Relative errors induced by internal coupling on the evaluation of the fractal dimension D_f and on the structure factor in the backscattering configuration for different refractive indices at $\lambda = 266$ nm.

Refractive index m	D_f error factors	Backscatter error factors
$m = 1.1 + i0.01$	0%	-1%
$m = 1.5 + i0.01$	0%	2%
$m = 1.9 + i0.01$	-1%	8%
$m = 1.1 + i0.4$	4%	-17%
$m = 1.5 + i0.4$	4%	-15%
$m = 1.9 + i0.4$	3%	-10%
$m = 1.1 + i0.8$	8%	-28%
$m = 1.5 + i0.8$	7%	-26%
$m = 1.9 + i0.8$	6%	-22%

The impact seems less sensitive to n than to $\mathrm{Im}\{m\} = \kappa$ but it contributes to an amplification of the effect of internal coupling on the optical structure factor.

Table 1 reports the errors induced by the internal coupling on the interpretation of the structure factor in terms of the fractal dimension D_f, i.e., the negative the slope measured in the power-law regime, and the specific value in backscattering. As for f_2, those parameters are governed by κ, while the role played by n seems to be less pronounced due to the contribution of f_1 that has to be considered for the determination of the resulting structure factor. However, it should be noted that the determination of D_f, which is based on the slope of the structure factor in the power-law regime, largely depends on the region considered for said slope measurement.

The bumps and the maximum deviations observed at 180° seen in Figs. 7 and 8 are morphology dependent. A different aggregate could yield different features. To investigate possible morphological dependence, we make use of the ergodicity theorem to abandon orientation averaging, and rather, average over 540 different DLCA aggregates taken from Yon et al. [41] with $N_m \in [10, 300]$, $D_f \approx 1.78$ and $k_f \approx 1.4$, and where each aggregate has an arbitrary fixed orientation.

As expected, when averaged over many different aggregates (see Fig. 9), the bumps disappear. A fit is proposed by an empirically chosen function $a \times \arctan(b \times x^c)$ with a, b, and c, respectively, equal to 0.133, 0.107, 2.122 for $m = 1.9 + i0.8$ and 0.095, 0.052, 2.695 for $m = 1.1 + i0.8$ for $\lambda = 266$ nm.

5. Conclusion

The RDG-FA approximation is commonly used for the modeling of the optical properties of fractal aggregates, including soot, and thus for the interpretation of light scattering measurements. However, its criteria are sometimes difficult to fulfill, especially for absorbing aerosols, and depend on the ratio between the primary-sphere diameter and wavelength. Those deviations have been numerically observed in the past and often attributed to internal coupling (or intra-cluster multiple scattering). Nevertheless, a precise

physical understanding of the phenomenon was lacking, in particular concerning the impact on the structure factor. Indeed, the structure factor, for many applications including SAXS experiments, is still evaluated as the Fourier transform of the autocorrelation function which is a pure morphological descriptor of the aggregate, and thus, internal coupling cannot be considered.

In this work, an optical autocorrelation function is introduced, which considers the non-uniformity of the internal electric field expressed in terms of phasors. It is demonstrated that the optical autocorrelation function is a complex function. The imaginary part of is at the origin of a new term in the expression of the structure factor written f_2 in this manuscript. The function's imaginary part explains the abnormal decrease of the structure factor at large scattering angles where internal coupling becomes relevant. This could impacts the optical determination of the aggregates fractal dimension made of absorbing material, in particular at lower wavelengths and could have a non-negligible impact on LIDAR measurements, i.e., for the backscattering configuration in presence of very large particles as superagregates [20]. We also show why the determination of the radius of gyration is not much impacted by internal coupling. Finally, it is demonstrated that structure-factor deviation is essentially driven by the phase shift of the light as it crosses the particle, induced by the internal trapping effect, which seems to be essentially driven by the imaginary part of the refractive index. Therefore, experimenters using UV light must take into account the possibility of large errors when dealing with optically absorbing materials with a size exceeding $qR_g > 3$. For example, backscatter errors of up to 28% for $qR_g \approx 10$ and up to 8% for the fractal dimension for a possible soot index $m = 1.1 + i0.8$ at $\lambda = 266\,\text{nm}$ are observed. The scale-invariant nature of the structure factor [45] makes it possible to extend some of the observations reported in this study to other wavelengths if the refractive index remains fixed; otherwise, the dispersion of the material must be taken into account. However, it should be noted that the amorphous and graphitic soot indices in [19], for the UV and near UV, are rather close. Indeed, κ does not vary strongly, and as seen here it is the cause of the main deviations. Concerning the indices in the IR range, the spectral dispersion is not necessarily a problem because unless the objects are very large, the structure factor will not go far enough in qR_g to measure the fractal dimension. Note that, this study has been performed for a specific fractal dimension ($D_f = 1.78$) and prefactor ($k_f = 1.40$) for point touching spheres. Therefore, others morphologies could affect the observations.

A perspective of this work would be to consider realistic aggregate morphologies by adding, for example, overlapping, necking, or coating to the monomers [46]. Indeed, such realistic objects have been shown to amplify the deviations from the RDG-FA [28,29] and associated depolarization effects [47], where the latter observation is well-known to be induced by internal coupling [48].

Declaration of Competing Interest

The authors declare that they have no known competing financial interests or personal relationships that could have appeared to influence the work reported in this paper.

Data availability

Data will be made available on request.

Acknowledgments

This work was financed by ANR ASTORIA (N° ANR-18-CE05-0015). The authors thank the CRIANN numerical resources supported by the Normandy, France region. CA thanks Josê Moran for providing a database of fractal aggregates. MB acknowledges support from the National Science Foundation, awards 1453987 and 1665456, the U.S. Air Force Office of Scientific Research awards FA9550-19-1-0078 and FA9550-21-1-0339, and the U.S. Army Research Office award FA9550-21-1-0339. RC acknowledges support from ONERA (PROMETE project).

References

[1] Boström C-E, Gerde P, Hanberg A, Jernström B, Johansson C, Kyrklund T, et al. Cancer risk assessment, indicators, and guidelines for polycyclic aromatic hydrocarbons in the ambient air. Environ Health Perspect 2002;110(suppl 3):451–88.
[2] Juarez-Facio AT, Castilla C, Corbire C, Lavanant H, Afonso C, Morin C, et al. Development of a standardized in vitro approach to evaluate microphysical, chemical, and toxicological properties of combustion-derived fine and ultrafine particles. J Environ Sci 2022;113:104–17. doi:10.1016/j.jes.2021.06.001. https://www.sciencedirect.com/science/article/pii/S1001074221002291
[3] Bond TC, Doherty SJ, Fahey DW, Forster PM, Berntsen T, DeAngelo BJ, et al. Bounding the role of black carbon in the climate system: a scientific assessment. J Geophys Res 2013;118(11):5380–552.
[4] Forrest SR, Witten TA. Long-range correlations in smoke-particle aggregates. J Phys A: Math Gen 1979;12(5):L109–17. doi:10.1088/0305-4470/12/5/008.
[5] Morán J, Yon J, Poux A. Monte carlo aggregation code (mcac) part 1: fundamentals. J Colloid Interface Sci 2020;569:184–94.
[6] Morán J, Yon J, Poux A, Corbin F, Ouf F-X, Siméon A. Monte carlo aggregation code (mcac) part 2: application to soot agglomeration, highlighting the importance of primary particles. J Colloid Interface Sci 2020;575:274–85.
[7] Sorensen CM. Light scattering by fractal aggregates: A Review. Aerosol Sci Technol 2001;35(2):648–87. doi:10.1080/02786820117868.
[8] Liu J, Zhang Q, Wang J, Zhang Y. Light scattering matrix for soot aerosol: comparisons between experimental measurements and numerical simulations. J Quant Spectrosc Radiat Transf 2020;246:106946.
[9] Yon J, Morán J, Lespinasse F, Escudero F, Godard G, Mazur M, et al. Horizontal planar angular light scattering (hpals) characterization of soot produced in a laminar axisymmetric coflow ethylene diffusion flame. Combust Flame 2021;232:111539.
[10] Beaucage G. Approximations leading to a unified exponential/power-Law approach to small-Angle scattering. J Appl Crystallogr 1995;28(6):717–28. doi:10.1107/S0021889895005292.
[11] Zhang F, Wang C, Han W, Zou Y, Wang J, Seifert S, et al. Soot formation and growth with palladium acetylacetonate-toluene injection in ethylene base flames investigated by in situ synchrotron small-angle x-ray scattering. Proc Combust Inst 2021;38(1):1859–66. doi:10.1016/j.proci.2020.10.004.
[12] Yon J, Ouf F-X, Hébert D, Mitchell JBA, Teuscher N, Le Garrec J-L, et al. Investigation of soot oxidation by coupling LII, SAXS and scattering measurements. Combust Flame 2018;190:441–53. doi:10.1016/j.combustflame.2017.12.014.
[13] Kerker M. The scattering of light and other electromagnetic radiation. Physical Chemistry: A Series of Monographs, vol. 16. Academic Press; 1969. doi:10.1016/C2013-0-06195-6.
[14] Bohren CF, Huffman DR. Absorption and scattering of light by small particles. John Wiley & Sons; 1983.
[15] Guinier A, Fournet G, Yudowitch KL. Small-angle scattering of. x-rays 1955.
[16] Porod G. Die röntgenkleinwinkelstreuung von dichtgepackten kolloiden systemen. Kolloid-Zeitschrift 1951;124(83):11435–536. doi:10.1007/BF01512792.
[17] Dobbins RA, Megaridis CM. Absorption and scattering of light by polydisperse aggregates. Appl Opt 1991;30(33):4747–54. doi:10.1364/AO.30.004747.
[18] Yon J, Liu F, Bescond A, Caumont-Prim C, Roze C, Ouf F-X, et al. Effects of multiple scattering on radiative properties of soot fractal aggregates. J Quant Spectrosc Radiat Transf 2014;133:374–81. doi:10.1016/j.jqsrt.2013.08.022.
[19] Sorensen CM, Yon J, Liu F, Maughan J, Heinson WR, Berg MJ. Light scattering and absorption by fractal aggregates including soot. J Quant Spectrosc Radiat Transf 2018;217:459–73.
[20] Ceolato R, Paulien L, Maughan JB, Sorensen CM, Berg MJ. Radiative properties of soot fractal superaggregates including backscattering and depolarization. J Quant Spectrosc Radiat Transf 2020;247:106940. doi:10.1016/j.jqsrt.2020.106940.
[21] Rannou P, McKay C, Botet R, Cabane M. Semi-empirical model of absorption and scattering by isotropic fractal aggregates of spheres. Planet Space Sci 1999;47(3):385–96. doi:10.1016/S0032-0633(99)00007-0.
[22] Yon J, Rozé C, Girasole T, Coppalle A, Méés L. Extension of rdg-fa for scattering prediction of aggregates of soot taking into account interactions of large monomers. Particle Particle Syst Character 2008;25(1):54–67.
[23] Lapuerta M, Gonzlez-Correa S, Cereceda-Balic F, Moosmller H. Comparison of equations used to estimate soot agglomerate absorption efficiency with the rayleigh-debye-gans approximation. J Quant Spectrosc Radiat Transf 2021;262:107522. doi:10.1016/j.jqsrt.2021.107522.
[24] Liu C, Yin Y, Hu F, Jin H, Sorensen CM. The effects of monomer size distribution on the radiative properties of black carbon aggregates. Aerosol Sci Technol 2015;49(10):928–40. doi:10.1080/02786826.2015.1085953.
[25] Prasanna S, Rivire P, Soufiani A. Effect of fractal parameters on absorption properties of soot in the infrared region. J Quant Spectrosc Radiat Transf 2014;148:141–55. doi:10.1016/j.jqsrt.2014.07.004.

[26] Liu F, Snelling DR, Smallwood GJ. Effects of the fractal prefactor on the optical properties of fractal soot aggregates. In: International Conference on Micro/Nanoscale Heat Transfer, vol. 43901; 2009. p. 363–71.
[27] Liu F, Wong C, Snelling DR, Smallwood GJ. Investigation of absorption and scattering properties of soot aggregates of different fractal dimension at 532nm using rdg and gmm. Aerosol Sci Technol 2013;47(12):1393–405. doi:10.1080/02786826.2013.847525.
[28] Yon J, Bescond A, Liu F. On the radiative properties of soot aggregates part 1: necking and overlapping. J Quant Spectrosc Radiat Transf 2015;162:197–206. doi:10.1016/j.jqsrt.2015.03.027.
[29] Liu F, Yon J, Bescond A. On the radiative properties of soot aggregates part 2: effects of coating. J Quant Spectrosc Radiat Transf 2016;172:134–45. doi:10.1016/j.jqsrt.2015.08.005.
[30] Brasil AM, Farias TL, Carvalho MG. Evaluation of the fractal properties of cluster-cluster aggregates. Aerosol Sci Technol 2000;33(5):440–54. doi:10.1080/02786820050204682.
[31] Argentin C, Berg MJ, Mazur M, Ceolato R, Yon J. Assessing the limits of rayleighdebye gans theory: phasor analysis of a bisphere. J Quant Spectrosc Radiat Transf 2021;264:107550. doi:10.1016/j.jqsrt.2021.107550.
[32] Argentin C, Berg MJ, Mazur M, Ceolato R, Poux A, Yon J. A semi-empirical correction for the rayleigh-debye-gans approximation for fractal aggregates based on phasor analysis: application to soot particles. J Quant Spectrosc Radiat Transf 2022;283:108143. doi:10.1016/j.jqsrt.2022.108143.
[33] Berg M, Sorensen C, Chakrabarti A. Explanation of the patterns in mie theory. J Quant Spectrosc Radiat Transf 2010;111(5):782–94. doi:10.1016/j.jqsrt.2009.11.010.
[34] Ceolato R, Berg MJ. Aerosol light extinction and backscattering: a review with a lidar perspective. J Quant Spectrosc Radiat Transf 2021;262:107492. doi:10.1016/j.jqsrt.2020.107492.
[35] Ceolato R, Bedoya-Velsquez A, Fossard F, Mouysset V, Paulien L, Lefebvre S, et al. Black carbon aerosol number and mass concentration measurements by picosecond short-range elastic backscatter lidar. Sci Rep 2022;12. doi:10.1038/s41598-022-11954-7.
[36] Romanov AV, Yurkin MA. Rigorous analysis of the spectral sizing of single particles based on light scattering patterns. Opt Laser Technol 2022;151:108047. doi:10.1016/j.optlastec.2022.108047.
[37] Draine B.T., Flatau P.J.. User guide for the discrete dipole approximation code ddscat 7.3. 2013. 10.48550/ARXIV.1305.6497
[38] Yurkin MA, Mishchenko MI. Volume integral equation for electromagnetic scattering: rigorous derivation and analysis for a set of multilayered particles with piecewise-smooth boundaries in a passive host medium. Phys Rev A 2018;97:043824. doi:10.1103/PhysRevA.97.043824.
[39] Draine BT, Flatau PJ. Discrete-dipole approximation for scattering calculations. J Opt Soc Am A 1994;11(4):1491–9. doi:10.1364/JOSAA.11.001491.
[40] Meakin P. Formation of fractal clusters and networks by irreversible diffusion-limited aggregation. Phys Rev Lett 1983;51(13):1119–22. doi:10.1103/PhysRevLett.51.1119.
[41] Yon J, Morn J, Ouf F-X, Mazur M, Mitchell J. From monomers to agglomerates: a generalized model for characterizing the morphology of fractal-like clusters. J Aerosol Sci 2021;151:105628. doi:10.1016/j.jaerosci.2020.105628.
[42] Yurkin M, Hoekstra A. The discrete dipole approximation: an overview and recent developments. J Quant Spectrosc Radiat Transf 2007;106(1):558–89. doi:10.1016/j.jqsrt.2007.01.034.
[43] Berg MJ, Sorensen CM. Internal fields of soot fractal aggregates. J Opt Soc Am 2013;30(10):1947–55. doi:10.1364/JOSAA.30.001947.
[44] Heinson W, Sorensen C, Chakrabarti A. A three parameter description of the structure of diffusion limited cluster fractal aggregates. J Colloid Interface Sci 2012;375(1):65–9. doi:10.1016/j.jcis.2012.01.062.
[45] Mishchenko MI. Scale invariance rule in electromagnetic scattering. J Quant Spectrosc Radiat Transf 2006;101(3):411–15. doi:10.1016/j.jqsrt.2006.02.047.
[46] Liu L, Schuster GL, Moosmller H, Stamnes S, Cairns B, Chowdhary J. Optical properties of morphologically complex black carbon aerosols: effects of coatings. J Quant Spectrosc Radiat Transf 2022;281:108080. doi:10.1016/j.jqsrt.2022.108080.
[47] Bescond A, Yon J, Girasole T, Jouen C, Rozé C, Coppalle A. Numerical investigation of the possibility to determine the primary particle size of fractal aggregates by measuring light depolarization. jqsrt 2013;126:130–9. doi:10.1016/j.jqsrt.2012.10.011.
[48] Lu N, Sorensen CM. Depolarized light scattering from fractal soot aggregates. Phys Rev E 1994;50:3109–15. doi:10.1103/PhysRevE.50.3109.